Combustion and Flame 269 (2024) 113710

Contents lists available at ScienceDirect

Combustion and Flame

journal homepage: www.sciencedirect.com/journal/combustion-and-flame

Towards predictive simplified chemical kinetics for hydrogen detonations

Fernando Veiga-López [a,*], Said Taileb [b], Ashwin Chinnayya [c], Josué Melguizo-Gavilanes [c,d]

[a] Aerolab, Research Institute of Physics and Aerospace Science, University of Vigo, Campus de Ourense, Ourense, 32004, Galicia, Spain
[b] Safran Tech, Magny-Les-Hameaux, France
[c] Institute Pprime, UPR 3346 CNRS, ISAE-ENSMA, Université de Poitiers, 86961, Futuroscope-Chasseneuil, France
[d] Shell Global Solutions B.V., Major Hazards Management, Energy Transition Campus, 1031 HW Amsterdam, The Netherlands

ARTICLE INFO

Keywords:
Detonation
Curvature
Simplified kinetics
Hydrogen

ABSTRACT

A methodology to develop predictive simplified kinetics schemes (one-step/three-step chain-branching) is presented in which detonation velocity-curvature ($D-\kappa$) curves computed with detailed thermochemistry are used as the fitting target aiming to capture the turning point of the curve (κ_{crit}). This was motivated by the similar trend observed between the κ_{crit} values obtained using the simplified schemes of Taileb et al. (2020), fitted using conventional methods, and the critical reactive layer heights for detonation propagation under yielding confinement (h_{crit}) reported by the same authors. Both updated schemes satisfactorily reproduce the target $D-\kappa$ curves and are used to (re)compute multidimensional cellular detonations propagating in channels and confined by inert layers. Simulations show a much better agreement with the results obtained with detailed kinetics for the detonation flow fields, cell sizes distributions, and h_{crit}. Moreover, it is observed that the average curvatures of the computed fronts are in line with those predicted by the $D-\kappa$ formulation, providing supporting evidence of the applicability of reduced order models for fast and inexpensive estimates of detonation limiting behaviors in safety studies.

Novelty and Significance Statement

The novelty of this research lies in proposing and testing an alternative methodology to determine the kinetics parameters of simplified kinetics schemes (1−step and 3−step) so that these retain the predictive capabilities of detailed kinetics. This is achieved by using detonation velocity-curvature curves ($D-\kappa$) as a fitting target. Conventional fitting procedures, such as targeting ignition delay times and/or matching ZND profiles have been shown to perform poorly in previous research. The new methodology shows significant improvements in the prediction of dynamic detonation parameters in ideal detonations such as cell sizes distributions, as well as in the prediction of the critical reactive layer heights for detonation propagation under yielding confinement (h_{crit}); a canonical configuration of interest to propulsion and industrial safety. For the latter, the new methodology yields h_{crit} for H_2-O_2 detonations of h_{crit} = 12 mm instead of 24 mm (with conventional methods), and h_{crit} = 8 mm instead of 20 mm, for the 1-step and 3-step models, respectively. The $D\kappa$ results are much closer to those obtained with detailed kinetics (h_{crit} = 6 mm) and to the experimental measurements (h_{crit} = 4.6 mm). The methodology is generic to be applied to any mixture of interest.

1. Introduction

One of the primary challenges in combustion modeling is the integration of chemistry. For example, a detailed mechanism for a typical hydrocarbon fuel used in transportation may include hundreds of species and thousands of reactions [1]. To address this issue, reduction techniques have been developed, which aim to maintain their predictive capabilities while minimizing the number of species and reactions. These techniques include quasi-steady state, directed graph, manifold, and genetic algorithms methods [2–4], as well as simpler systematic approaches based on error metrics [5].

The turbulent combustion community has led most of these efforts, likely driven by industrial needs [6,7], both in stationary and mobile energy conversion systems, to conceive more fuel-efficient and less polluting alternatives. On the contrary, the detonation community has lacked such drivers and has been historically satisfied with a mostly qualitative understanding of the phenomenon given by the simplest descriptions of the chemistry (i.e., one-step Arrhenius). This is due in part to the very stringent resolution requirements to adequately resolve multidimensional detonation fronts. In actuality, when predictions/data are needed for limiting behaviors (i.e., detonability limits, detonation

* Corresponding author.
E-mail address: fernando.veiga@uvigo.gal (F. Veiga-López).

https://doi.org/10.1016/j.combustflame.2024.113710
Received 31 January 2024; Received in revised form 28 August 2024; Accepted 29 August 2024
Available online 6 September 2024

initiation/diffraction, and quenching), experimental databases continue to be the most reliable source [8], although some success has been achieved recently when coupling inviscid hydrodynamic solvers with H_2-O_2 detailed kinetics (9 species/21 reactions) [9,10].

The integration of more complex fuels is expected to remain prohibitively expensive in the near future. Therefore, a good compromise would be to develop simplified kinetic schemes that can reproduce quantitatively the limiting behaviors mentioned above. Some past and recent efforts on simplified modeling for detonation applications include one- to five-step schemes developed with varying degrees of sophistication [11–19]. One common feature present in detonation initiation, propagation, and diffraction is that their fronts are observed to be globally curved. Conventional fitting procedures, however, rely on using the laminar planar ZND structure hoping to reproduce the complex thermodynamic changes and associated chemical rates in the induction zone of multidimensional detonations. As discussed below, kinetic schemes fitted in this way (or variations thereof such as targeting constant pressure/volume induction times over a temperature and pressure range of interest) not only fail at predicting the minimum reactive layer height for detonation propagation under yielding confinement (h_{crit}) [9] but also at capturing one of the simplest extensions to the ZND model (i.e., quasi-steady weakly-curved detonation waves), the so-called $D-\kappa$ curves.

It is natural to expect that fitting the rates of simplified schemes to capture the critical curvatures predicted by detailed mechanisms would result in simplified kinetics that reproduce more closely the expected chemical rates in the reaction zone at dynamic sub-D_{CJ} conditions.

In this work, a methodology in which $D-\kappa$ curves obtained with detailed kinetics are used as the fitting target is presented (Sect. 2). Results using the new approach and conventional methods are compared and discussed for ideal and non-ideal detonation propagation (Sect. 3). Closing remarks are included in Sect. 4.

2. Fitting methodology

2.1. Physical model

2.1.1. Governing equations

The generalized quasi-steady ZND model, which considers weakly curved leading shock fronts, can be derived by adding source/sink terms to the reactive Euler equations as described in [20] and other seminal works on the topic [21–24].

$$\frac{\mathrm{d}\rho}{\mathrm{d}x} = -\frac{\rho}{\mathrm{w}}\frac{(\dot{\sigma}-\mathrm{w}(1-\eta)\alpha)}{\eta}, \tag{1}$$

$$\frac{\mathrm{dw}}{\mathrm{d}x} = \frac{(\dot{\sigma}-\mathrm{w}\alpha)}{\eta}, \tag{2}$$

$$\frac{\mathrm{d}p}{\mathrm{d}x} = -\rho\mathrm{w}\frac{(\dot{\sigma}-\mathrm{w}\alpha)}{\eta}, \tag{3}$$

$$\frac{\mathrm{d}Y_k}{\mathrm{d}x} = \frac{W_k\dot{\omega}_k}{\rho\mathrm{w}} \quad (k=1,\ldots,N), \tag{4}$$

$$\dot{\sigma} = \sum_{k=1}^{N}\left(\frac{\overline{W}}{W_k}-\frac{h_k}{c_pT}\right)\frac{\mathrm{d}Y_k}{\mathrm{d}t},$$

$$\alpha = \frac{1}{A}\frac{\mathrm{d}A}{\mathrm{d}x} = \kappa\left(\frac{D}{\mathrm{w}}-1\right),$$

where, ρ, w, p, and t are the mixture density, axial velocity in the wave-attached frame, pressure, and time, respectively. The mass fraction, molecular weight and net production/consumption rates per unit mass of species k are given by Y_k, W_k and $\dot{\omega}_k$. Here $\eta = 1-M^2$ is the sonic parameter and $M = \mathrm{w}/a_f$ is the Mach number relative to the leading shock computed using the frozen speed of sound, a_f. $\dot{\sigma}$ is the thermicity, α the axial area change representing the flow divergence that is related to the shock curvature. $\overline{W}$ is the mean molar mass of the mixture, c_p the mixture specific heat at constant pressure, and h_k is the specific enthalpy of species k. Finally, κ is the curvature of the wave front given by $2/R_c$ for spherical waves, and $1/R_c$ for cylindrical waves with R_c being the local radius of curvature; see [20] for additional details. It can be readily shown that setting $\alpha = 0$ reverts the formulation to the ideal case included in Browne et al. [25]. The implementation in the Shock and Detonation Toolbox (SDT) [25] only entails adding the terms containing α, making it rather straight forward, and most importantly, allowing us to investigate arbitrary chemical mechanisms written in Cantera format [26] (i.e., *.cti* files). The numerical root-finding algorithm developed by Veiga-López et al. [27] for detonations with friction was adapted to handle weakly curved detonations. The model has been used successfully in previous work that investigated the influence of low temperature chemistry on steady detonations with curvature losses [28,29].

2.1.2. Chemistry modeling

The chemistry is modeled using the same methodology presented in Taileb et al. [9], namely, chemical schemes of increasing complexity: single-step, three-step chain-branching and detailed kinetics [30]. For completeness, the most salient features and assumptions made in the simplified schemes are briefly described next.

In the single-step model, the fuel, F, is directly converted into products following a single irreversible Arrhenius reaction, $F \rightarrow P$, occurring at a rate $k = A_s\exp(-E_a/R_uT)$. In the three-step chain-branching model, *initiation*, *branching* and *termination* steps are accounted for that mimic the initial thermally neutral decomposition of the fuel (F) to produce active radicals (R) at rate r_I, the subsequent abrupt increase of the radical pool at rate r_B, and their final conversion into products (P) at rate r_T accompanied by heat release, respectively.

Initiation: F (Fuel) $\rightarrow R$ (Chain-carriers),

$$r_I = k_I(\rho/\overline{W})Y_F\exp\left(\frac{-E_I}{R_uT}\right), \tag{5}$$

Branching: $F + R \rightarrow 2R$,

$$r_B = k_B(\rho/\overline{W})^2Y_FY_R\exp\left(\frac{-E_B}{R_uT}\right), \tag{6}$$

Termination: $R \rightarrow P$ (Products),

$$r_T = k_C(\rho/\overline{W})Y_R, \tag{7}$$

where E_I/R_u and E_B/R_u are the activation temperatures, and $k_I = k_C\exp(E_I/R_uT_I)$, $k_B = k_C\,(W/\rho_{vN})\exp(E_B/R_uT_B)$ and k_C are the pre-exponential factors; ρ_{vN} is the von Neumann density.

The additional degrees of freedom in the latter model (i.e., initiation/branching activation energies and cross-over temperatures) allow for increased flexibility to reproduce more complex chemical behaviors such as the sensitivity of hydrogen auto-ignition to initial temperature/pressure, and the distinction between induction and reaction zone and their respective length-scales. For all the simplified chemical schemes, the reactive mixture is assumed to have a constant mean molar mass, $\overline{W}$, ratio of specific heats, $\gamma = c_p/c_v$, and total heat release, Q; see [9] for further details and the implications of these assumptions. The detailed mechanism of Mével et al. [30] (9 species and 21 reactions) whose predictions had been shown to provide sensible results when compared against experiments [9,10] is used to compute the reference curves. It should be noted that measurable variations are anticipated based on the specific detailed chemical kinetics chosen [27] the so-called *mechanism-induced uncertainties* which are outside of the scope of the current work. Therefore, the predictive capabilities of the simplified models discussed here are restricted to those of the reference mechanism selected.

2.2. $D-\kappa$ curves

Fig. 1 (left) shows the $D-\kappa$ curves obtained for a stoichiometric H_2-O_2 mixture at ambient pressure and temperature using the chemical models described above, and the same kinetic parameters as in Taileb et al. [9]: $A_s = 1.1\times10^9$ s^{-1}, and $E_a/R_u = 11277$ K, for single-step kinetics; and $k_C = 2\times10^7$ s^{-1}, $E_I/R_u = 25000$ K, $E_B/R_u = 9300$ K,

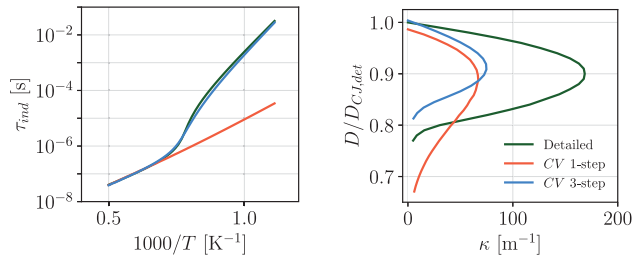

Fig. 1. Constant volume induction times, τ_{ind} at ρ_{vN} (left) and $D-\kappa$ curves (right) obtained with detailed chemistry [30] and the CV schemes. $D_{CJ,det}$ is the steady propagation velocity computed with detailed chemistry. Conditions: stoichiometric H_2-O_2 at $p_0 = 100$ KPa and $T_0 = 300$ K. .

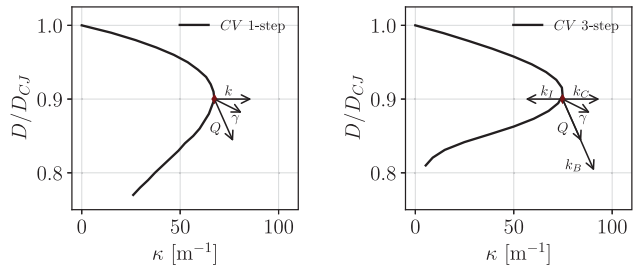

Fig. 2. Influence of the thermodynamic and kinetic parameters on the calculated $D-\kappa$ curves for single-step (left) and three-step chain-branching kinetics (right). The size of the arrows qualitatively indicates how sensitive the turning point of the curve is to changes in each parameter.

$T_I = 2431$ K, $T_B = 1430$ K, for three-step chain-branching kinetics. These are referred to as/labeled CV 1-step and CV 3-step, respectively. The γ and Q values characterizing the reactive mixture are given in Table 1.

Fig. 1 clearly shows that simplified mechanisms fitted to reproduce the constant volume induction times of detailed kinetics, as was done in [9] (Fig. 1-left), yield significantly different turning points, i.e., κ_{crit} (Fig. 1-right). More interesting is the fact that the κ_{crit} obtained ($\kappa_{crit,1\text{-step}} = 67.4$ m^{-1}; $\kappa_{crit,3\text{-step}} = 74.8$ m^{-1}; $\kappa_{crit,det} = 168.5$ m^{-1}) follows the same trend as that of the 2-D simulations of Taileb et al. [9] where the critical reactive layer heights, h_{crit}, for detonation propagation under yielding confinement were determined; a higher critical front curvature yields a lower h_{crit}. To compare with their results a crude estimate for the curvature defined as $\kappa_{eq} \propto 1/h_{crit}$ is used: $\kappa_{eq,1\text{-step}} = 41.7$ m^{-1}; $\kappa_{eq,3\text{-step}} = 50.0$ m^{-1} $\kappa_{eq,detailed} = 166.7$ m^{-1}. Note that in both cases, $\kappa_{1\text{-Step}} < \kappa_{3\text{-step}} \ll \kappa_{Detailed}$. This last observation may imply, and will be confirmed later, that using κ_{crit} as a fitting target for the development of simplified schemes could result in improved predictive capabilities in multidimensional simulations.

2.3. κ_{crit} as fitting target

Fig. 2 shows the effect of varying the thermodynamic and kinetic parameters of the simplified schemes on the resulting $D-\kappa$ curves. The size of the arrows qualitatively indicates how sensitive the turning point of the curve is to changes in each parameter. Note that this is consistent with [31,32] for the 1-step case. For the modified mechanisms, the initial conditions were improved over those in [9] by matching as best as possible the steady detonation velocity, D_{CJ}, and von Neumann temperature, T_{vN}, computed with detailed kinetics. This entailed finding the best combination of Q and γ within realistic values for stoichiometric H_2-O_2 detonations while ensuring that the proper velocity deficits for increasing κ were captured, as well as the turning point of the curves, κ_{crit}.

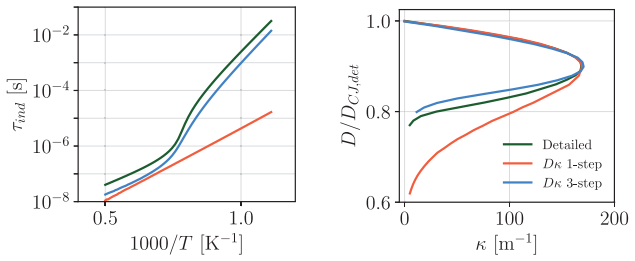

Fig. 3. Constant volume induction times, τ_{ind} at ρ_{vN} (left) and $D-\kappa$ curves (right) obtained with the $D\kappa$ schemes and compared with detailed kinetics results. Conditions: stoichiometric H_2-O_2 at $p_0 = 100$ KPa and $T_0 = 300$ K.

The parameters found after the manual trial-and-error fitting exercise are included in Table 1 as well as detonation properties of interest to the discussion. Bear in mind that only A_s and k_C were modified whereas the initiation/branching activation energies and cross-over temperatures were left unchanged as these are more appropriately defined in ignition delay time vs. inverse temperature plots. Note that the slopes in the high- and low-temperature regimes and the temperature threshold at which the change of activation energy occurs do not change, there is only a shift along the y-axis consistent with the increase of the rate multipliers (see Fig. 3-left). Changes in the available degrees of freedom should always be guided by the thermochemical behavior of the mixture of interest. This method ensures that the induction time and reaction zone length are matched reasonably well to those obtained with the detailed chemistry.

The updated $D-\kappa$ curves are shown in Fig. 3-right. In agreement with the large activation energy asymptotics in [20]: (i) given fixed thermodynamic conditions and E_a/R_u, higher reaction rates k result in larger κ_{crit} values; (ii) an increase in T_{vN}, given by the new thermodynamics (i.e., Q and γ), yields a decrease in $D(\kappa_{crit})$ and an increment in κ_{crit}. Both simplified schemes reproduce quite well the expected behavior for $D/D_{CJ,det} > D/D_{CJ,det}(\kappa_{crit})$. However, significant deviations are present for larger deficits. The differences in the computed velocity deficits $D/D_{CJ,det}$ at fixed κ using detailed/three-step chain-branching kinetics when compared with those of one-step in the range $D/D_{CJ,det} < 0.9$ are a consequence of the known inability of the one-step models to adequately reproduce the H_2-O_2 ignition delay times at post-shock temperatures below the chain-branching cross-over temperature (see Fig. 3- right). Nonetheless, this does not seem to be a first order effect for improved predictions of h_{crit} in multidimensional simulations; capturing κ_{crit} will be shown to provide much better estimates than the reference simplified kinetics used in [9]. The schemes fitted with the methodology described above will be referred to as/labeled $D\kappa$ 1-step and $D\kappa$ 3-step hereinafter.

3. Results and discussion

3.1. Ideal 1-D steady structure

The ZND profiles obtained with the CV (left) and $D\kappa$ (right) schemes are compared with those using detailed kinetics in Fig. 4. It can be seen that the modified simplified schemes reproduce much better the von Neumann state, which was one of the fitting objectives. Moreover, the induction lengths, l_{ind}, obtained with the updated reduced kinetics vary considerably because the modified pre-exponential factors always increased during the fitting, and the resulting combination of Q and γ required to yield higher T_{vN}, ultimately sped up the chemical reaction. For instance, the $D\kappa$ 3-step scheme, resulted in a l_{ind} that is $\sim 48\%$ smaller than that predicted by the detailed mechanism. Note that matching l_{ind} was not a target nor a constraint of the proposed fitting procedure, which aimed to find a parameter combination that captured

Table 1
Detonation and thermodynamic properties for a stoichiometric H_2-O_2 mixture for all chemical schemes used. The pre-exponential factors for simplified kinetics are also shown. Initial conditions: $p_0 = 100$ kPa and $T_0 = 300$ K.

Chemical model	D_{CJ} [m/s]	T_{vN} [K]	$\gamma_{(0-vN-CJ)}$	Q [MJ/kg]	A_s ; k_C [s^{-1}]	l_{ind} [μm]	$E_{a,eff}/R_uT_o$
Detailed kinetics [30]	2839.9	1768.7	1.4 – 1.315 – 1.218	–	–	41	28.78
CV 1-step [9]	2801.5	1674.8	1.33	4.800	6.0×10^9	87.9	33.99
Dκ 1-step	2836.9	1769.5	1.35	4.606	1.08×10^{10}	36.2	35.92
CV 3-step [9]	2850.4	1723.7	1.33	4.990	2.0×10^7	46.8	30.83
Dκ 3-step	2836.2	1768.7	1.35	4.613	4.0×10^7	21.4	30.08

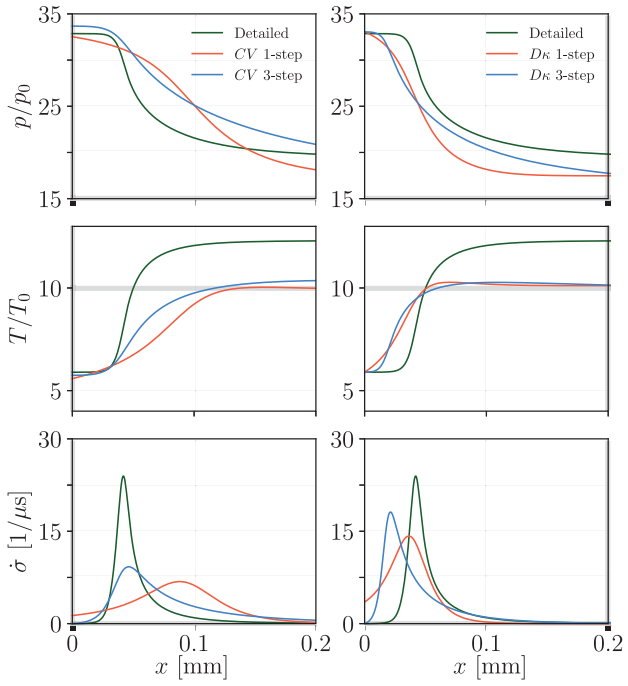

Fig. 4. ZND profiles - Pressure, temperature and thermicity obtained with the *CV* (left) and *Dκ* (right) schemes. The ZND profiles computed with detailed chemistry [30] are included as a reference.

the critical curvature obtained with the quasi-steady 1-D model. The CJ state position (i.e., $\dot{\sigma} \rightarrow 0$) better matched that predicted by the detailed chemistry. However, the thermodynamic conditions at this state strongly differ from the detailed mechanism due to the constant γ assumption. Therefore, all simplified models do not account for changes in the molecular weight of the gas between the fresh mixture and the products. The χ parameter [33] given by $\chi = (E_{a,eff}/R_uT_{vN}) \cdot l_{ind} \cdot \dot{\sigma}_{max}/u_{CJ}$ where $\dot{\sigma}_{max}$ denotes the maximum in the thermicity profile, can be computed solely based on ZND profiles, and is reported in Table 2. This metric is often used to characterize cellular structure regularity. Section 3.2 will show that χ does not seem to be as relevant in our case for predicting changes in cellular structure probably due to the fact that their values remain relatively similar. The effective activation energy seems to better predict the changes in the nature of the cellular structure (i.e., higher $E_{a,eff}/R_uT_o$ values yielding more irregular flow fields). Furthermore, Section 3.3 will show that h_{crit} bears no correlation with χ which suggests a key role of multidimensional effects in its determination.

Finally, while it is plausible that several combinations of the fitting parameters (*i.e.*, γ, Q, A_S and k_C) may lead to simplified schemes that would match κ_{crit} in $D-\kappa$ curves, it is outside of the scope of this work to provide the optimal combination. Rather, a novel fitting approach for simplified kinetics is presented and systematically evaluated.

Table 2
χ parameter [33] computed with the different chemical mechanisms.

Chemical model	χ
Detailed kinetics [30]	3.187
CV 1-step [9]	2.270
Dκ 1-step	1.875
CV 3-step [9]	1.389
Dκ 3-step	1.177

3.2. Ideal 2-D propagation in channels

The parallel in-house code RESIDENT (REcycling mesh SImulations of DEtoNaTions) was used to integrate the Euler equations in 2-D with a uniform mesh ($\Delta x = \Delta y = l_{ind}/10$ pts). A detonation was initiated and allowed to propagate in a channel completely filled with stoichiometric H_2-O_2 at $p_0 = 100$ kPa and $T_0 = 300$ K until a quasi-steady structure was achieved. A sliding window technique was used to follow the detonation as it propagated into mixture at rest [34]. This allowed us to have a fixed number of cells in the computational domain at all times, irrespective of the length of the channel computed. Detailed descriptions of the numerical methods employed in RESIDENT for spatial and temporal discretizations as well as the parallelization strategy can be found in [34,35]. The instantaneous flow fields, the numerical soot foils and average and local front curvatures are analyzed once the detonation reaches a velocity close to the ideal Chapman-Jouguet speed, D_{CJ} (to within ±2%). Following this approach, it is possible to avoid any influence of the initiation transient. Note that this is the same numerical methodology used in the work by Taileb et al. [9] so that a meaningful comparison can be performed. RESIDENT has been previously used in fundamental detonation studies using simplified [36] and detailed chemical kinetics [9,37] for ideal and non-ideal gases [38].

3.2.1. Instantaneous flow fields

Fig. 5 shows the instantaneous temperature and normalized density gradient fields of the detonations obtained with the reference (*CV*) and new (*Dκ*) simplified schemes; results with the detailed chemical mechanism are also included as a reference. The *Dκ* schemes yield fields that are qualitatively much closer to the detailed mechanism, albeit exhibiting a lower final average temperature because of the constant molecular weight assumption discussed earlier. The combined effect of (i) enhanced resilience to curvature, which allows the front to locally fold further without quenching, and (ii) the presence of stronger transverse waves that leads to a sharper density gradient behind the shock compared to the detonations computed in [9], yield more homogeneous flow fields and reduce the amount of unburned pockets present when the *Dκ* schemes are used. Furthermore, the visibly more irregular detonation fields obtained with the *Dκ* 1-step are directly related to its higher effective activation energy, $E_{a,eff}/R_uT_o$, when compared to that of detailed chemistry (see Table 1).

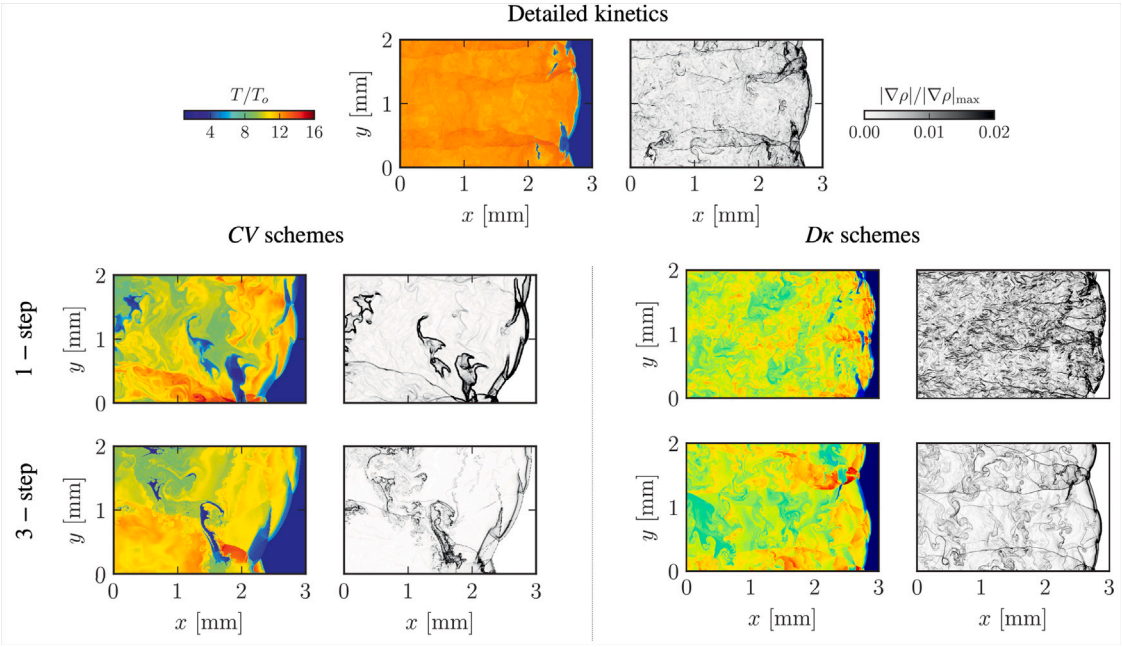

Fig. 5. Instantaneous temperature and normalized density gradient fields obtained with detailed chemistry [30], *CV* and *Dκ* schemes.

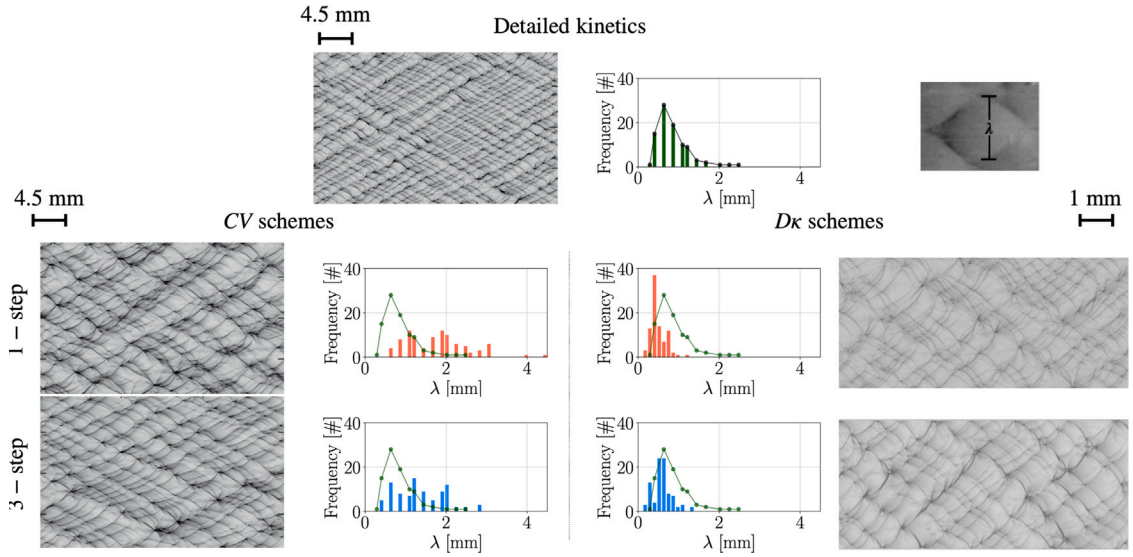

Fig. 6. Numerical soot foils and cell-size histograms obtained with detailed chemistry [30], *CV* and *Dκ* schemes. Note the differences in scale among the soot foils. A schematic showing the length that is typically referred to as the cell size λ is also included.

3.2.2. Numerical soot foils and cell size histograms

Fig. 6 includes a schematic of the length that is typically referred to as the cell size λ, the numerical soot foils and the cell size histograms for all the chemical schemes tested. Oblong cells are measured from bottom-to-top vertex. The sample size is fixed to 90 and the size of the cells is measured manually from the soot foils and counting the number of times, i.e. *frequency*, a range of cell size appears. The histograms show that the cell size distributions are significantly better predicted by the *Dκ* schemes. The latter yield smaller cells ($\lambda_{\text{max},\,CV,\ \text{1-step}} = 1.8$ mm vs. $\lambda_{\text{max},\,D\kappa,\ \text{1-step}} = 0.4$ mm; $\lambda_{\text{max},\,CV,\ \text{3-step}} = 1.2$ mm vs. $\lambda_{\text{max},\,D\kappa,\ \text{3-step}} = 0.57$ mm) that were in much closer agreement to those estimated by the detailed chemical mechanism ($\lambda_{\text{max, detailed}} = 0.6$ mm). The reduction in cell sizes can be explained by the faster rates required in the $D-\kappa$ schemes and associated reduction in l_{ind}.

3.3. Non-ideal 2-D propagation

Further analysis is carried out by computing 2-D detonations confined by an inert layer. This canonical configuration is of interest to novel propulsion applications such as rotating detonation engines (RDEs) [39–41], as well as safety since upon a fuel leak into open space and subsequent ignition of the resulting reactive cloud a detonation may be initiated [42]. Again, the same numerical setup as in [9] is used and, for completeness, briefly summarized next. Once a detonation at D_{CJ} is stabilized in an ideal channel, the upstream conditions are modified to include an inert layer in the domain. The size of the inert layer, measured from the top of the domain, is progressively increased at a constant step ($\Delta h = 2$ mm) resulting in a thinner reactive layer of thickness h. At a certain height the detonation quenches before reaching $x_Q = x - x_{0,\,\text{inert layer}}$ where $x_{0,\,\text{inert layer}}$ is the axial position at

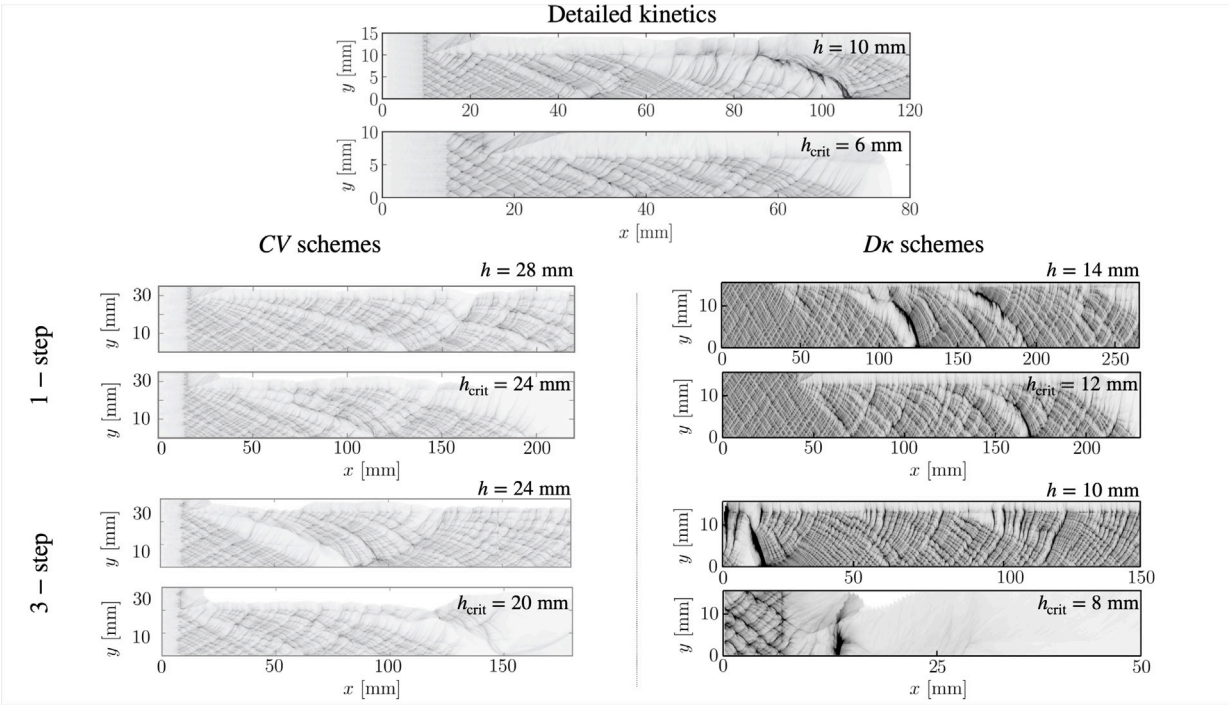

Fig. 7. Numerical soot foils for detonation waves propagating through reactive layers heights of $h = h_{crit} + \Delta h$ and $h = h_{crit}$ for detailed chemistry [30], *CV* and *Dκ* schemes.

which the ideal detonation meets the inert layer, and x_Q the distance at which the cellular pattern fades completely. The x_Q values reported in [9] at h_{crit} are used as a reference to determine quenching. Once again, the reader is referred to [9] for further details about the initial and boundary conditions used. It should be noted that one simulation is run every time the reactive height h is changed, which makes finding h_{crit} a computationally expensive process.

3.3.1. Critical heights prediction

The *Dκ* schemes h_{crit} predictions are discussed next. Table 3 shows the results of the simulations. The *Dκ* schemes yield lower h_{crit} values than the *CV* schemes, i.e., h_{crit} = 12 mm instead of 24 mm, and h_{crit} = 8 mm instead of 20 mm, for the 1-step and 3-step models, respectively. Note that the *Dκ* results are much closer to those obtained with detailed kinetics (h_{crit} = 6 mm) and to the experimental measurements (h_{crit} = 4.6 mm). Therefore, it seems that κ_{crit} is a valid fitting target to develop simplified schemes with improved predictive capabilities. Put differently, adding the physics expected to play an important role as part of the fitting procedure helps to properly capture important gas dynamical and chemical features thereby improving the predictive capabilities in simulations of multidimensional detonations.

The numerical soot foils for representative cases are included in Fig. 7. These show the complex dynamics of the interaction between the detonation and the inert layer prior and during quenching. The presence of strong expansions partially quench and curve the detonation close to the interface; transverse waves and their reflections at the lower wall re-initiate the detonation. A more thorough description of the propagation and quenching dynamics for this configuration was already provided in [9].

3.3.2. Average and local front curvature at $h > h_{crit}$

Due to the interaction with the inert layer and the lateral expansion of burnt gases, the leading shock curves. Fig. 8 depicts steady detonation fronts propagating through a reactive layer slightly higher than h_{crit} (i.e, $h = h_{crit} + \Delta h$; note that Δh used here differs from that used in [9]). The *Dκ* schemes allow more curved detonations to propagate without quenching through thinner layers, because of faster

Table 3
Critical heights predicted by the different chemical schemes.

Chemical scheme	h_{crit} [mm]	x_Q [mm]
Detailed kinetics [30]	6	60
CV 1-step [9]	24	200
Dκ 1-step	12	176
CV 3-step [9]	20	140
Dκ 3-step	8	12
Experimental [43]	4.6	–

reaction rates required to match κ_{crit} than those in the *CV* schemes. The weak global curvature assumption invoked in the $D-\kappa$ model, used to fit the chemistry herein, is justified by the 2-D flow fields obtained. Interestingly, these fields also provide the means to assess to which extent the actual 2-D front curvatures can be compared with the κ_{crit} value given by the $D-\kappa$ model.

The 2-D detonation front average and local curvatures are obtained by fitting a second and fifth order polynomial, respectively, to the plane curve $f(x, y)$ given by the maximum of the normalized density gradient which delineates the front. The curvature is subsequently computed using $\kappa = |x'y'' - y'x''| \cdot \left(x'^2 + y'^2\right)^{-3/2}$ where the prime notation, $'$ and $''$, represent first and second derivatives. Analytical differentiation was used in the function evaluation.

Fig. 9 shows the average and local curvature of the propagating fronts. A few things are worth mentioning regarding the values of the local curvature as these are sensitive to: (i) the smoothing used on the initially noisy line that delineates the detonation front, and (ii) the order of the polynomial chosen to fit the detonation front. The results show that the local curvatures can attain values as high as $\kappa_{loc,\,2\text{-D}} \sim 250$ m^{-1}; this is ~ 4 times larger than the curvature given by the $D-\kappa$ model for a detonation propagating at $D \sim 0.96 D_{CJ}$, that is, $\kappa_{1\text{-D}} \sim 70$ m^{-1}. Conversely, the average curvature $\kappa_{avg,\,2\text{-D}} \sim 50$ m^{-1} is comparable to $\kappa_{1\text{-D}}$. This observation provides supporting evidence that $\kappa_{avg,\,2\text{-D}}$ serves as a more representative metric to compare against the results of the $D-\kappa$ model. It is worth mentioning that Reynaud et al. [35] used a more sophisticated method to compute

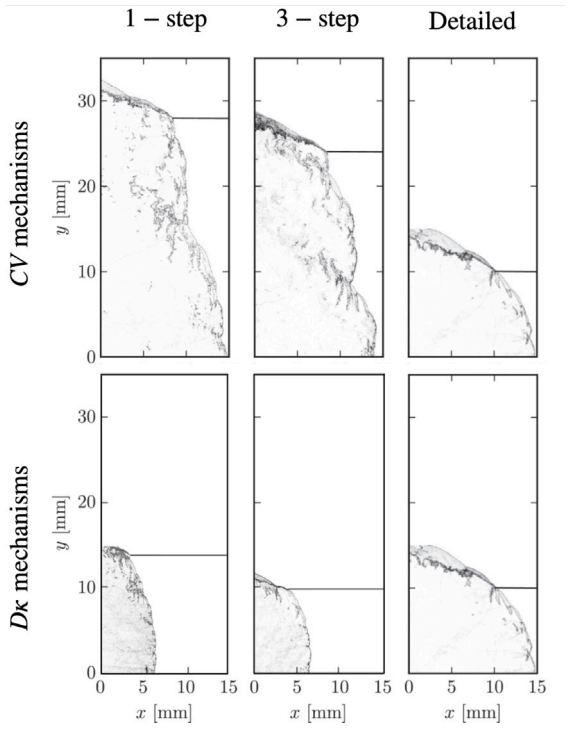

Fig. 8. Normalized density gradient fields obtained for detonations propagating through reactive layer heights of $h = h_{crit} + \Delta h$ computed with detailed chemistry [30], *CV* and *Dκ* schemes.

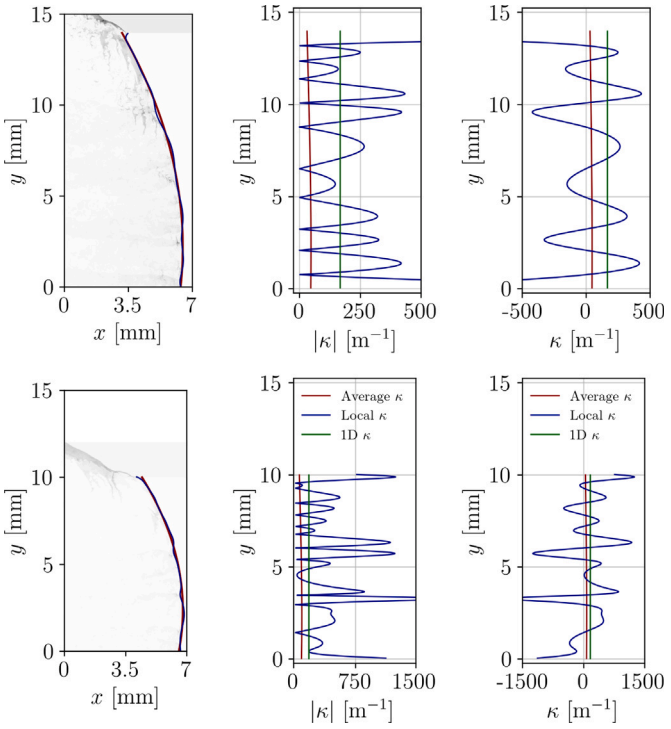

Fig. 9. Normalized density gradient fields obtained for detonations propagating through layers of $h = h_{crit} + \Delta h$ for the *Dκ* 1-step (top) and *Dκ* 3-step (bottom). Absolute $|\kappa|$ and signed κ value of local (blue) and average (red) curvatures measured from the instantaneous fields are shown. 1D κ (green) denotes the value of κ_{crit} obtained from the $D - \kappa$ model.

global/average and local curvatures, argued to be more relevant to general detonation dynamics, which entailed time-averaging the flow field at the lower wall.

3.3.3. *Curvature-driven quenching dynamics at $h = h_{crit}$*

The fronts curve more close to the inert layer where the expansion waves originate from than at the vicinity of the lower wall. As a result, the detonation wave slows down and eventually quenches as $h \to h_{crit}$. In Fig. 10, the curvatures of the detonation fronts prior to quenching are given. The local curvatures are, as expected, higher than those for $h > h_{crit}$ ($\kappa_{loc,\,2\text{-}D} \sim 500$ m^{-1}); the average curvatures ($\kappa_{avg,\,2\text{-}D} \sim 70$ m^{-1}) are again similar to the estimates of the $D - \kappa$ model for a velocity deficit of $D \sim 0.95 D_{CJ}$ ($\kappa_{1\text{-}D} \sim 100$ m^{-1}).

The temporal quenching dynamics of the *Dκ* schemes are analyzed in detail in Fig. 11 for $h \geq h_{crit}$. This is carried out measuring the variation of the average instantaneous curvature of the fronts as a function of time, the diamond-shaped marker indicates the time at which quenching occurred. Note that a similar convention to that used to determine the quenching location x_Q above, is used here to define the quenching time $t - t_0$, that is, time is measured relative to the moment the detonation wave meets the inert interface, t_0.

For the *Dκ* 1-step scheme (Fig. 11 - left), the detonation propagating in a reactive layer height of $h = h_{crit} + \Delta h = 14$ mm experiences a smooth increase in curvature immediately after interaction with the inert layer. Upon reaching a value of $\kappa_{2\text{-}D} \sim 35$ m^{-1} the curvature decreases and an oscillatory phase starts, in which folding and stretching of the front takes place. At $t - t_0 \sim 32.5$ µs, $t - t_0 \sim 50$ µs and $t - t_0 \sim 82.5$ µs, the detonation exhibits a strong sudden increase in its curvature, yielding local quenching at $x \sim 110$ mm, $x \sim 170$ mm and $x \sim 240$ mm, respectively, in agreement with the soot foils of Fig. 7. In this case, the detonation front re-initiates due to the presence of strong transverse waves/triple points that reflect off the bottom wall, originating from the interface with the inert layer. For $h = h_{crit} = 12$ mm, the dynamics are essentially the same: the front curves when the detonation interacts

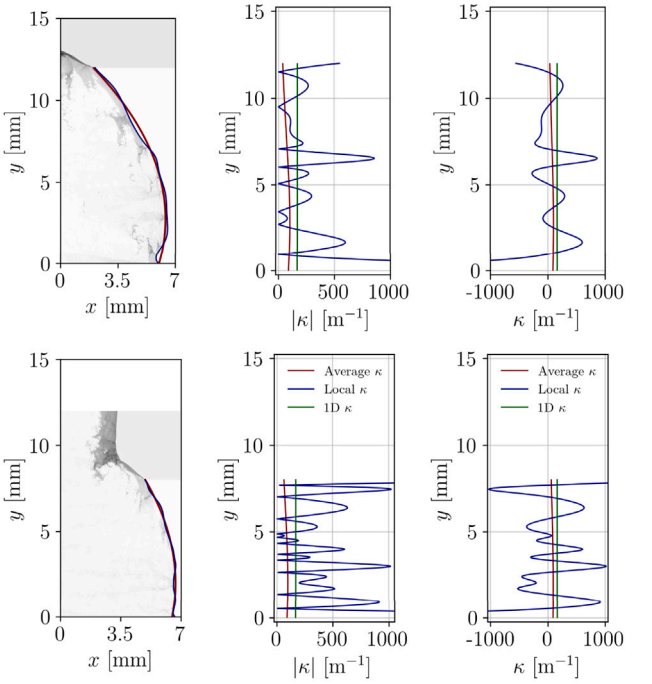

Fig. 10. Normalized density gradient fields obtained for detonations propagating through layers of $h = h_{crit}$ for the *Dκ* 1-step (top) and *Dκ* 3-step (bottom). Absolute $|\kappa|$ and signed κ value of local (blue) and average (red) curvatures measured from the instantaneous fields are shown. 1D κ (green) denotes the value of κ_{crit} obtained from the $D - \kappa$ model.

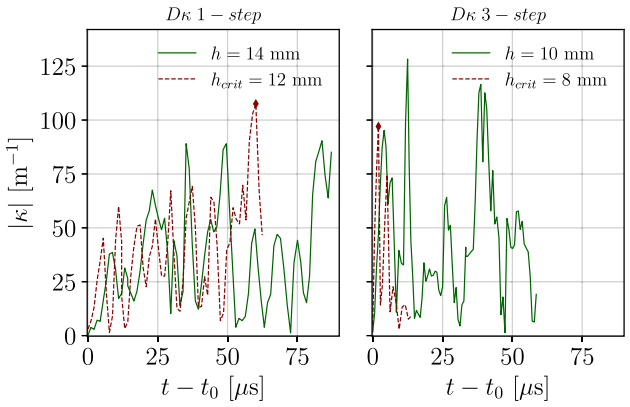

Fig. 11. Temporal evolution of the average curvature of the detonation front profiles measured from interaction with the inert layer ($t = t_0$). The red diamond-shaped markers represent the quenching point for reactive layer heights of $h = h_{\text{crit}}$.

with the inert layer, and an oscillatory phase in the curvature of the front ensues, causing local extinction/re-initiation. However, at a certain point, the front curvature reaches a value of $\kappa_{\text{crit, 2-D}} \sim 110$ m^{-1}, which quenches the detonation fully; no re-initiations were observed thereafter.

For the $D\kappa$ 3-step scheme (Fig. 11 - right), the detonation front exhibits similar dynamics as that described above for propagation in a reactive layer height of $h = h_{\text{crit}} + \Delta h = 10$ mm. In this particular case, the oscillations are not as regular. This is due to the very strong curvature increase at around $t - t_0 \sim 12$ µs and $t - t_0 \sim 40$ µs, that results in locally strong quenching events followed by re-initiations. For $h = h_{\text{crit}} = 8$ mm, the detonation quenches shortly after interacting with the inert layer. The sudden increase of curvature around $\Delta\kappa \sim 100$ m^{-1}, and associated expansion, effectively decouples the front and the chemical energy release; no re-initiation attempts were observed in this case.

While the propagation and quenching dynamics observed for the $D\kappa$ 1-step and $D\kappa$ 3-step schemes were quite different at $h = h_{\text{crit}}$, they do share a common feature. The detonations locally/globally quench whenever the average curvature reaches a value around $\kappa_{\text{2-D}} > 100$ m^{-1} provided that the transverse waves present are not strong enough to reactivate chemical reactions and re-initiate the front. Note that the critical curvatures and velocity deficits the $D-\kappa$ model yield, $\kappa_{\text{crit, 1-D}} \sim 167$ m^{-1} and $D/D_{CJ}(\kappa_{\text{crit}}) = 0.9$, are of the same order of magnitude as those computed from the 2-D fields. The quantitative discrepancies just reported are not necessarily surprising given the $D - \kappa$ model assumptions, and indicates that unsteadiness/deceleration [44] of the front as well as its multidimensional structure play an important role in the quenching dynamics. In spite of this, the results seem to suggest that low-order models may still serve as fast and inexpensive tools to estimate reactive layer heights (i.e., limiting behaviors) in RDE design and safety relevant scenarios, at least for the case of H_2 detonations.

Finally, note that the h_{crit} predicted by the $D\kappa$ 1-step and $D\kappa$ 3-step differ even though they share the same 1-D fitting target. Two reasons come to mind. First, the conception of the simplified 1-/3-step schemes irrespective of their fitting target (i.e., CV or $D\kappa$). 3-step schemes provide a single pathway for the build-up radicals, if this pathway is stopped, there will be very little heat release to sustain the detonation wave. The latter occurs when $T < T_B$ suddenly stopping the production of chain-branching species. As previously explained, the initial transient upon interaction with the inert layer results in very high local curvatures that lead to thermodynamic states within the above mentioned temperature range ultimately resulting in prompt decoupling of the leading shock and reaction zone. On the other hand, 1-step schemes are less sensitive because the chemistry is always active in the postshock region. As a result, these are not capable of reproducing the thermally neutral l_{ind} nor of mimicking the change in activation energy typical of H_2 mixtures. 1-step schemes always result in unrealistically short induction times for $T < T_B$; see Fig. 1-left. Second, the differences in l_{ind} and the much slower energy deposition in the flow for the $D\kappa$ 1-step mechanism, rendering it less effective to reproduce realistic detonation behaviors; see $\dot{\sigma}$ profiles in Fig. 4. The above may also explain the differences in the quenching distances, x_Q, reported in Table 3. Finally, while it could be argued that the reduction in h_{crit} may be fundamentally due to a reduction in l_{ind}, it has been shown in previous work [9] that capturing l_{ind} alone does not lead to an adequate prediction of h_{crit}. Note that the l_{ind} that is used as a fitting target in conventional methods usually comes from a single ZND wave propagating at D_{CJ}. A key aspect that the current study reveals is the crucial role that curvature plays during detonation quenching and the importance of properly capturing the reactivity changes as the wave gets weakened and curved by expansion waves thereby decoupling the leading shock from the reaction zone while propagating at sub-D_{CJ} speeds. Therefore, the evidence so far seems to suggest that it is the more adequate chemical response of the wave to curvature losses that leads to better predictive capabilities. This is precisely what using the $D - \kappa$ model with κ_{crit} as a fitting target allows us to do in a relatively straightforward fashion.

4. Conclusion

Simplified kinetics schemes obtained by fitting the critical curvature predicted by the $D - \kappa$ curves obtained with detailed chemistry are proposed ($D\kappa$ schemes). These were used to compute ideal and non-ideal detonation propagation in 2-D. Of special interest was the determination of the critical reactive layer height that leads to quenching, h_{crit}. The results were compared to those reported in Taileb et al. [9] in which simplified kinetics fitted by matching the constant volume induction times (CV schemes) given by the same detailed mechanism were used. Results show that the $D\kappa$ schemes yield front structures that are qualitatively and quantitatively more similar to those given by detailed chemistry (i.e., cell size histograms and lower h_{crit} values) thus in better agreement with experimental measurements. Including the physics expected to play a role in the quenching process (curvature effects) as part of the fitting procedure, resulted in simplified schemes with improved predictive capabilities over standard methods. The methodology is generic and can be applied to any mixture of interest. Furthermore, detonations interacting with inert layers are found to follow an oscillatory change in their curvature when $h \to h_{\text{crit}}$: the fronts stretch and fold up to a critical curvature that impedes their propagation. Future work will include testing/extending the proposed fitting procedure to H_2-O_2 mixtures away from stoichiometry, H_2-air and hydrocarbons; the development of a thermodynamically consistent methodology for predictive simplified kinetics is the object of current research efforts [19].

CRediT authorship contribution statement

Fernando Veiga-López: Writing – review & editing, Writing – original draft, Methodology, Investigation. **Said Taileb:** Writing – review & editing. **Ashwin Chinnayya:** Writing – review & editing. **Josué Melguizo-Gavilanes:** Writing – review & editing, Investigation, Funding acquisition, Conceptualization.

Declaration of competing interest

The authors declare that they have no known competing financial interests or personal relationships that could have appeared to influence the work reported in this paper.

Acknowledgments

Financial support from the Agence Nationale de la Recherche Program JCJC (FASTD ANR-20-CE05-0011-01) is gratefully acknowledged. Computations were carried out at the supercomputer facilities of the Mésocentre de Calcul de Poitou-Charentes and using HPC resources from GENCI-CINES (Grant A0152B07735). F. Veiga-López is grateful to Universidade de Vigo, Spain for their financial support for Open Access publication.

References

[1] H. Wang, E. Dames, B. Sirjean, D.A. Sheen, R. Tangko, A. Violi, J.Y.W. Lai, F.N. Egolfopoulos, D.F. Davidson, R.K. Hanson, C.T. Bowman, C.K. Law, W. Tsang, N.P. Cernansky, D.L. Miller, R.P. Lindstedt, A high-temperature chemical kinetic model of *n*-alkane (up to *n*-dodecane), cyclohexane, and methyl-, ethyl-, *n*-propyl and *n*-butyl-cyclohexane oxidation at high temperatures, 2010, JetSurF version 2.0. URL http://web.stanford.edu/group/haiwanglab/JetSurF/JetSurF2.0/index.html.

[2] J. Van Oijen, F. Lammers, L. De Goey, Modeling of complex premixed burner systems by using flamelet-generated manifolds, Combust. Flame 127 (2001) 2124–2134.

[3] P. Pepiot, H. Pitsch, Systematic reduction of large chemical mechanisms, in: 4th Joint Meeting of the US Sections of the Combustion Institute, Philadelphia, PA, 2005, pp. 324–330.

[4] J.J. Hernández, R. Ballesteros, J. Sanz-Argent, Reduction of kinetic mechanisms for fuel oxidation through genetic algorithms, Math. Comput. Modelling 52 (2010) 1185–1193.

[5] S. Coronel, J. Melguizo-Gavilanes, D. Davidenko, R. Mével, J. Shepherd, Reduction methodology for detailed kinetic mechanisms: application to n-hexane-air hot surface ignition, in: Asia Pacific Combustion Conference, Vol. 11, 2017.

[6] A. Felden, L. Esclapez, E. Riber, B. Cuenot, H. Wang, Including real fuel chemistry in LES of turbulent spray combustion, Combust. Flame 193 (2018) 397–416.

[7] W. Zheng, C. Kaplan, R. Houim, E. Oran, Flame acceleration and transition to detonation: Effects of a composition gradient in a mixture of methane and air, Proc. Combust. Inst. 37 (2019) 3521–3528.

[8] M. Kaneshige, J.E. Shepherd, Detonation Database, California Institute of Technology, 1997.

[9] S. Taileb, J. Melguizo-Gavilanes, A. Chinnayya, Influence of the chemical modeling on the quenching limits of gaseous detonation waves confined by an inert layer, Combust. Flame 218 (2020) 247–259.

[10] J. Melguizo-Gavilanes, V. Rodriguez, P. Vidal, R. Zitoun, Dynamics of detonation transmission and propagation in a curved chamber: A numerical and experimental analysis, Combust. Flame 223 (2021) 460–473.

[11] B. Varatharajan, M. Petrova, F. Williams, V. Tangirala, Two-step chemical-kinetic descriptions for hydrocarbon–oxygen-diluent ignition and detonation applications, Proc. Combust. Inst. 30 (2005) 1869–1877.

[12] M. Short, J.J. Quirk, On the nonlinear stability and detonability limit of a detonation wave for a model three-step chain-branching reaction, J. Fluid Mech. 339 (1997) 89–119.

[13] Z. Liang, L. Bauwens, Cell structure and stability of detonations with a pressure-dependent chain-branching reaction rate model, Combust. Theor. Model. 9 (2005) 93–112.

[14] Z. Liang, S. Browne, R. Deiterding, J. Shepherd, Detonation front structure and the competition for radicals, Proc. Combust. Inst. 31 (2007) 2445–2453.

[15] C.R. Kaplan, A. Özgen, E.S. Oran, Chemical-diffusive models for flame acceleration and transition-to-detonation: genetic algorithm and optimisation procedure, Combust. Theor. Model 23 (1) (2019) 67–86.

[16] X. Lu, C.R. Kaplan, E.S. Oran, A chemical-diffusive model for simulating detonative combustion with constrained detonation cell sizes, Combust. Flame 230 (2021) 111417.

[17] S. Taileb, E. Rougon, V. Robin, V. Rodriguez, P. Vidal, S. Lau-Chapdelaine, J. Melguizo-Gavilanes, A. Chinnayya, A three-step, three-gamma model for the numerical modeling of the critical height of the propagation of semi-confined detonation waves, in: 28th International Colloquium on the Dynamics of Explosions and Reactive Systems, 2022.

[18] M. Peswani, B. Maxwell, Detonation wave diffraction in stoichiometric C_2H_4/O_2 mixtures using a global four-step combustion model, Phys. Fluids 34 (2022).

[19] A. Millan-Merino, S.T. Taileb, F. Veiga-Lopez, J. Melguizo-Gavilanes, P. Boivin, A thermodynamically consistent methodology to develop predictive simplified kinetics for detonation simulations, in: International Conference of Hydrogen Safety, 2023.

[20] R. Klein, J.C. Krok, J. Shepherd, Curved Quasi-Steady Detonations: Asymptotic Analysis and Detailed Chemical Kinetics, California Institute of Technology, 1995, URL https://authors.library.caltech.edu/51558/1/FM95-4.pdf.

[21] Y.B. Zel'dovich, B. Gel'Fand, Y.M. Kazhdan, S. Frolov, Detonation propagation in a rough tube taking account of deceleration and heat transfe, Combust. Explo. Shock+ 23 (1987) 342–349.

[22] J.B. Bdzil, D.S. Stewart, Modeling two-dimensional detonations with detonation shock dynamics, Phys. Fluids A 1 (7) (1989) 1261–1267.

[23] J.B. Bdzil, D.S. Stewart, The dynamics of detonation in explosive systems, Annu. Rev. Fluid Mech. 39 (1) (2007) 263–292.

[24] J. Saenz, B. Taylor, D. Stewart, Asymptotic calculation of the dynamics of self-sustained detonations in condensed phase explosives, J. Fluid Mech. 710 (2012) 166–194.

[25] S. Browne, J. Ziegler, J. Shepherd, Numerical solution methods for shock and detonation jump conditions, in: GALCIT report FM2006, Citeseer, 2008, p. 90.

[26] D.G. Goodwin, R.L. Speth, H.K. Moffat, B.W. Weber, Cantera: An object-oriented software toolkit for chemical kinetics, thermodynamics, and transport processes, 2021, http://dx.doi.org/10.5281/zenodo.4527812, https://www.cantera.org. Version 2.5.1.

[27] F. Veiga-López, L.M. Faria, J. Melguizo-Gavilanes, Influence of chemistry on the steady solutions of hydrogen gaseous detonations with friction losses, Combust. Flame 240 (2022) 112050.

[28] F. Veiga-López, Z. Weng, R. Mével, J. Melguizo-Gavilanes, Influence of low-temperature chemistry on steady detonations with curvature losses, Proc. Combust. Inst. 39 (2023) 2925–2933.

[29] Z. Weng, F. Veiga-López, J. Melguizo-Gavilanes, R. Mével, Effect of ozone addition on curved detonations, Combust. Flame 247 (2023) 112479.

[30] R. Mével, J. Sabard, J. Lei, N. Chaumeix, Fundamental combustion properties of oxygen enriched hydrogen/air mixtures relevant to safety analysis: Experimental and simulation study, Int. J. Hydrog. Energy 41 (2016) 6905–6916.

[31] L. He, P. Clavin, On the direct initiation of gaseous detonations by an energy source, J. Fluid Mech. 277 (1994) 227–248.

[32] M.I. Radulescu, J.H. Lee, The failure mechanism of gaseous detonations: experiments in porous wall tubes, Combust. Flame 131 (2002) 29–46.

[33] H.D. Ng, Y. Ju, J.H. Lee, Assessment of detonation hazards in high-pressure hydrogen storage from chemical sensitivity analysis, Int. J. Hydrog. Energy 32 (2007) 93–99.

[34] M. Reynaud, F. Virot, A. Chinnayya, A computational study of the interaction of gaseous detonations with a compressible layer, Phys. Fluids 29 (2017) 056101.

[35] M. Reynaud, S. Taileb, A. Chinnayya, Computation of the mean hydrodynamic structure of gaseous detonations with losses, Shock Waves 30 (2020) 645–669.

[36] M. Faghih, J. Melguizo-Gavilanes, R. Mével, A modified Lotka–Volterra oscillating chemical scheme for detonation simulation, Combust. Flame 254 (2023) 112827.

[37] K.P. Chatelain, R. Mével, J. Melguizo-Gavilanes, A. Chinnayya, S. Xu, D.A. Lacoste, Effect of incident laser sheet orientation on the OH-PLIF imaging of detonations, Shock Waves 30 (7-8) (2020) 689–702.

[38] S. Taileb, J. Melguizo-Gavilanes, A. Chinnayya, The influence of the equation of state on the cellular structure of gaseous detonations, Phys. Fluids 33 (3) (2021).

[39] D. Schwer, K. Kailasanath, Numerical investigation of rotating detonation engines, in: 46th AIAA/ASME/SAE/ASEE Joint Propulsion Conference & Exhibit, 2010, p. 6880.

[40] S. Frolov, A. Dubrovskii, V. Ivanov, Three-dimensional numerical simulation of operation process in rotating detonation engine, Prog. Propuls. Phys. 4 (2013) 467–488.

[41] C.A. Nordeen, D. Schwer, F. Schauer, J. Hoke, T. Barber, B. Cetegen, Thermodynamic model of a rotating detonation engine, Combust. Explos. Shock Waves 50 (2014) 568–577.

[42] J. Melguizo-Gavilanes, M. Peswani, B. Maxwell, Detonation-diffuse interface interactions: failure, re-initiation and propagation limits, Proc. Combust. Inst. 38 (2021) 3717–3724.

[43] E.K. Dabora, J. Nicholls, R. Morrison, The influence of a compressible boundary on the propagation of gaseous detonations, in: Symp. Combust. Proc., vol. 10, Elsevier, 1965, pp. 817–830.

[44] J. Shepherd, Ignition Modeling and the Critical Decay Rate Concept, Technical Report, California Institute of Technology, 2020, EDL2019-002. URL https://shepherd.caltech.edu/EDL/publications/reprints/cdr_modelEDL2019-002.pdf.